Progress In Electromagnetics Research C, Vol. 173, 256–265, 2026
PIER C

(Received 30 July 2026, Accepted 8 September 2026, Scheduled 14 September 2026)

Improved Terminal Sliding Mode Control for PMSM Dual-Inertia System Based on Dual Finite-Time Disturbance Observers

Jinyang Zou[1], Kaihui Zhao[1,*], Gang Fan[2,*], Kai Shen[2], and Lin Jia[1]

[1]*School of Transportation and Electrical Engineering, Hunan University of Technology, China*
[2]*School of Rail Transit Locomotives, Hunan Railway Professional Technology College, China*

ABSTRACT: To address speed-tracking degradation and torsional vibration caused by flexible-shaft coupling and load disturbances in PMSM dual-inertia systems, this paper proposes a high-order nonsingular fast integral terminal sliding mode control (HONFITSMC) method integrated with dual finite-time extended sliding mode disturbance observers (FTESMDOs). First, a third-order load-side dynamic model is derived to explicitly describe the effects of shaft torque and load disturbance. Next, the HONFITSMC method is developed using an inner integral sliding surface, an outer high-order sliding surface, and a dual-power reaching law. Furthermore, a weighting function is introduced to adapt the convergence speed across different error regions, reducing chattering and improving speed-tracking accuracy. Then, dual FTESMDOs are designed for the motor side and load side to estimate the shaft torque and load-side disturbances, and the estimated values are fed forward into the control law for real-time compensation. The simulated and experimental results demonstrate that the proposed control scheme significantly improves the system's disturbance rejection capability and overall robustness.

1. INTRODUCTION

High-performance servo systems based on permanent magnet synchronous motors (PMSMs) are widely used in robotics, computer numerical control (CNC) machining, aerospace, and other industries that require precision [1, 2]. These systems typically incorporate transmission components, such as drive shafts, gearboxes, and couplings, which connect the motor to the load. These systems are often referred as dual-inertia systems. They typically exhibit nonlinear disturbances, such as friction and backlash. These disturbances can cause resonance and degrade the control performance.

Various control strategies have been proposed by researchers to improve system performance, including active disturbance rejection control (ADRC) [3], proportional-integral (PI) control [4], model predictive control (MPC) [1], and sliding mode control (SMC) [5]. Among them, the conventional linear SMC is the most widely used. This is because it offers strong robustness, fast dynamic response, and excellent disturbance rejection capability. However, its switching function is not continuous. This can easily cause system chattering, which can then excite mechanical resonance in a flexible transmission system [6]. Meanwhile, the system states on a conventional linear sliding surface typically converge asymptotically. This makes it difficult to meet the fast dynamic response requirements of high-performance servo systems.

To overcome the asymptotic convergence of the conventional SMC, terminal SMC (TSMC) [7] achieves finite-time convergence by introducing nonlinear power terms into the sliding surface. However, conventional TSMC may suffer from singularity when the system state approaches the equilibrium point. Nonsingular terminal SMC (NTSMC) was therefore developed to avoid this problem [8]. Fast terminal SMC (FTSMC) [9] was subsequently introduced to improve the convergence speed when the system state is far from or close to the equilibrium point. Integral terminal SMC (ITSMC) [10] was also developed to improve the transient response and initial robustness. Yang et al. [11] combined fast integral terminal SMC with an iterative learning-based disturbance observer to improve speed-tracking and disturbance-rejection performance of a PMSM drive system. However, its capability to handle parameter perturbations and time-varying load disturbances has not been fully verified. Lu et al. [12] proposed a model-free recursive terminal SMC method with a double-disturbance observer for a PMSM dual-inertia system.

In PMSM dual-inertia flexible transmission systems, speed tracking behavior of the load side is affected jointly by load disturbances, parameter perturbations, and flexible shaft torque coupling. To address this issue, disturbance observers (DOs) [13] and extended state observers (ESOs) [14] have been widely used to estimate unknown dynamics and external disturbances. The estimated disturbances can then be introduced into the controller for feedforward compensation. However, the performance of conventional DOs and ESOs depends strongly on model uncertainties, observer bandwidth, and parameter selection. A higher observer bandwidth may improve the response to fast disturbances, but it may also increase sensitivity to measurement noise. Extended sliding mode disturbance observers (ESMDO) treat the unknown disturbance as an extra state. They are more robust to bounded uncertainties than linear observers. However, their discontinuous injection terms can cause chattering in the disturbance

* Corresponding authors: Kaihui Zhao (zhaokaihui@hut.edu.cn); Gang Fan (496557710@qq.com).

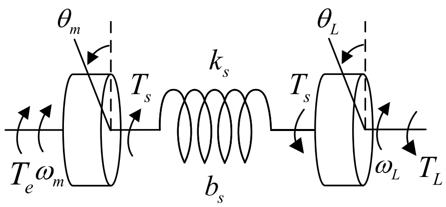

FIGURE 1. Model of a two-inertia system.

estimate. The ESMDO in [15] improves the estimation performance. Nevertheless, the rigorous finite-time convergence of the disturbance estimation error has not been explicitly established.

To address load-side speed tracking and torsional vibration suppression in the flexible shaft of a PMSM dual-inertia flexible transmission system, this paper presents a high-order fast integral terminal SMC (HONFITSMC) method based on dual finite-time extended sliding mode disturbance observers (FTESMDOs). The proposed method is compared with proportional-integral (PI) control and the extended sliding mode disturbance observer (ESMDO)-based non-singular fast terminal SMC (NFTSMC) method. The results verify its effectiveness in tracking load-side speed, reducing torsional vibration of the flexible shaft, and compensating for load disturbances. The main contributions of this study are as follows:

(i) We develop HONFITSMC and FTESMDOs for the PMSM dual-inertia system. The HONFITSMC controller improves load-speed tracking and torsional vibration suppression, while the dual FTESMDOs estimate and compensate for motor-side and load-side disturbances. Their coordinated operation improves the disturbance rejection capability and system robustness.

(ii) We improve the controller by introducing an inner integral sliding surface, an outer high-order sliding surface, a weighted terminal function, and a dual-power reaching law. These modifications improve the convergence speed in different error regions and enhance load-speed tracking and torsional vibration suppression.

(iii) We derive a third-order load-side dynamic model and analyze the stability of the proposed control system under bounded disturbances. Subsequently, we verify the effectiveness and performance advantages of the proposed method through comparative simulations and experiments.

This paper is organized as follows. Section 2 derives the load-side dynamic model. Section 3 designs the HONFITSMC controller and proves its stability. Section 4 develops dual FTESMDOs and analyzes their stability. Section 5 validates the proposed method using comparative simulations and experiments. Finally, Section 6 summarizes the paper.

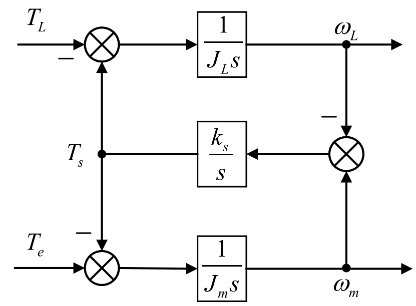

FIGURE 2. Structure of a two-inertia system.

2. MATHEMATICAL MODELING OF PMSM DUAL-INERTIA SYSTEMS

This section introduces relevant definitions, formulates a model of a PMSM dual-inertia flexible transmission system, and obtains the load-side dynamic model.

In a PMSM dual-inertia flexible transmission system, the motor side experiences electromagnetic torque and shaft torque. When the connecting device between the motor and load sides is elastic, it undergoes elastic deformation because the load side experiences shaft torque and load torque. This results in inconsistent rotational speeds between the system's motor and load sides. Figure 1 shows the model of the dual-inertia system, and Figure 2 shows the structural block diagram of the dual-inertia system.

Ignoring core saturation, neglecting eddy current and hysteresis losses, and assuming no parameter mismatch, the mathematical model of the PMSM dual-inertia system in the d-q axis reference frame is

$$\begin{cases} \frac{\mathrm{d}i_d}{\mathrm{d}t} = -\frac{R_s}{L_d}i_d - n_p\omega_m i_q + \frac{u_d}{L_d} \\ \frac{di_q}{dt} = -\frac{R_s}{L_q}i_q - n_p\omega_m i_d - \frac{n_p\psi_r}{L_q}\omega_m + \frac{u_q}{L_q} \\ \frac{d\omega_m}{dt} = \frac{1}{J_m}\left[\frac{3}{2}n_p\psi_r i_q - T_s - b_m\omega_m\right] \\ \frac{d\omega_l}{dt} = \frac{1}{J_L}\left(T_s - T_L - b_L\omega_l\right) \\ T_s = b_s\left(\omega_m - \omega_l\right) + k_s\left(\theta_m - \theta_l\right) \end{cases} \tag{1}$$

where u_d, u_q, i_d, and i_q represent stator voltages and currents along d and q axes, respectively; L_d and L_q denote stator inductances along d and q axes; R_s is the stator resistance; ψ_r is the permanent magnet flux linkage; ω_m and ω_e are mechanical and electrical angular velocities on the motor side, with $\omega_e = n_p\omega_m$; ω_l is the mechanical angular velocity on the load side; θ_m and θ_l are mechanical angles of the motor and load, respectively; J_m and J_L are the motor's moments of inertia and load respectively; k_s is the torsional stiffness of the coupling shaft; b_s is the torsional damping coefficient of the coupling shaft; n_p is the number of pole pairs; b_m and b_l are friction coefficients of the motor and load, respectively; T_s is the shaft torque; and T_L is the load torque. For a surface-mounted PMSM, $L_d = L_q$, and the electromagnetic torque is $T_e = 1.5n_p\psi_r i_q$.

Assumption 1 *The system's initial state is a stationary state, that is,* $\omega_m(0) = 0$, $\omega_L(0) = 0$, $T_s(0) = 0$. *The load-side* *reference speed and its first, second, and third derivatives are piecewise continuous and bounded.*

Assumption 2 *All parameter perturbations, external disturbances, and unmodeled dynamics in the system are bounded. Moreover, the first derivatives of the disturbances on the equivalent motor and load side are piecewise continuous and bounded.*

The effects of parameter perturbations, friction, and unmodeled dynamics are represented by disturbance terms d_m and d_L. Since the viscous damping coefficients b_m and b_L are negligible, the dual-inertia system can be simplified as follows:

$$\begin{cases} J_m\dot{\omega}_m = T_e - T_s + d_m \\ J_L\dot{\omega}_L = T_s - T_L + d_L \\ \dot{T}_s = K_s(\omega_m - \omega_L). \end{cases} \tag{2}$$

where $d_m = -\Delta J_m\dot{\omega}_m + \tau_m$, $d_L = -\Delta J_L\dot{\omega}_L + \tau_L$. Symbols ΔJ_m and ΔJ_L denote inertia perturbations, and symbols τ_m and τ_L denote external disturbances or unmodeled terms.

3. DESIGN OF HONFITSMC

This section presents the HONFITSMC method based on an improved double power reaching law and proves its stability. Subsequently, a controller was designed to achieve closed-loop control of the load speed in the PMSM dual-inertia system.

Taking the third-order derivative of the load speed Equation (2) yields:

$$\dddot{\omega}_L = \frac{K_s}{J_mJ_L}\left[T_e - \left(1 + \frac{J_m}{J_L}\right)T_s + \frac{J_m}{J_L}T_L\right] + \Delta_r \tag{3}$$

where $\Delta_r = \frac{K_s}{J_mJ_L}d_m - \frac{K_s}{J_L^2}d_L - \frac{1}{J_L}\ddot{T}_L + \frac{1}{J_L}\ddot{d}_L$. From Assumption 2, it follows that $|\Delta_r| \le \bar{\Delta}_r$.

Define the load-side speed tracking error as:

$$e = \omega_l - \omega_l^*. \tag{4}$$

Theorem 1 *Define the weighted terminal function*

$$\begin{aligned} f_1(S_\omega) &= \rho(S_\omega)\mathrm{sign}(S_\omega)|S_\omega|^p \\ &\quad + [1 - \rho(S_\omega)]\,\mathrm{sign}(S_\omega)\,|\mathrm{asinh}(S_\omega)|^p \end{aligned} \tag{5}$$

where $\rho(S_\omega) = \frac{|S_\omega|^r}{|S_\omega|^r + \delta^r}$, $0 < p < 1$, $r > 0$, $\delta > 0$. *If* $f_1(S_\omega)$ *satisfies* $f_1(0) = 0$, $S_\omega f_1(S_\omega) > 0$, $S_\omega \neq 0$, *then in a neighborhood of the origin, there exist positive constants* c_1 *and* c_2 *such that*

$$c_1|S_\omega|^p \le |f_1(S_\omega)| \le c_2|S_\omega|^p. \tag{6}$$

Proof 1 *For* $S \neq 0$, *we have*

$$|f_1(S)| = \rho(S)|S|^p + [1 - \rho(S)]|\mathrm{asinh}(S)|^p, \tag{7}$$

where the two terms on the right side of (7) have the same sign as S. *Because* $\mathrm{asinh}(S) = S + O(S^3)$ $(S \to 0)$, *we have* $\frac{|\mathrm{asinh}(S)|^p}{|S|^p} \to 1$ $(S \to 0)$.

Therefore, there exist a neighborhood $\mathcal{U}$ *and constants* $m, M > 0$ *such that*

$$m \le \frac{|\mathrm{asinh}(S)|^p}{|S|^p} \le M, \qquad S \in \mathcal{U}. \tag{8}$$

Since $0 \le \rho(S) \le 1$, *there exist positive constants* c_1, c_2 *such that* $c_1|S_\omega|^p \le |f_1(S_\omega)| \le c_2|S_\omega|^p$.

Select the inner integral sliding surface S_ω and outer high-order sliding surface sliding surface l_ω:

$$\begin{cases} S_\omega = \dot{e}_\omega + c_1e_\omega + c_2\int e_\omega dt \\ l_\omega = \dot{s}_\omega + \int_0^t(\gamma f_1 + \beta f_2)dt \end{cases} \tag{9}$$

where f_1 has been defined in Theorem 1. $f_2 = \mathrm{sign}(\dot{s}_\omega)\cdot|\dot{s}_\omega|^q$, $c_1 > 0$, $c_2 > 0$, $\gamma > 0$, $\beta > 0$, $\rho(S_\omega) = \frac{|S_\omega|^r}{|S_\omega|^r + \delta^r}$, $0 < p < 1$, $q = \frac{2p}{1+p}$, $r > 0$, $\delta > 0$.

Differentiating l_ω gives:

$$\dot{l}_\omega = \ddot{s}_\omega + \gamma f_1 + \beta f_2 \tag{10}$$

The improved dual power reaching law [16] is selected

$$u_{sw} = k_1(|S_\omega||l_\omega|)^{1-\alpha_1}\,\mathrm{sign}(l_\omega) + k_2|l_\omega|^{1+\alpha_1}\,\mathrm{sign}(l_\omega) \tag{11}$$

where $k_1 > 0$, $k_2 > 0$, $0 < \alpha_1 < 1$.

Combining (1), (3), (10), and (11) yields the control law:

$$i_q^* = \frac{2}{3n_p\psi_r}\left[-\frac{J_mJ_L}{K_s}u + \left(1 + \frac{J_m}{J_L}\right)\hat{D}_m - \frac{J_m}{J_L}\hat{D}_L\right] \tag{12}$$

where $u = c_1\ddot{e}_\omega + c_2\dot{e} + \gamma f_1 + \beta f_2 + u_{sw}$. The uncertain terms are represented as follows: the motor-side disturbance, $D_m = T_s - d_m$, and the load-side disturbance, $D_L = T_L - d_L$. $\hat{D}_m$ and $\hat{D}_l$ are disturbances on motor and load sides, respectively.

Lemma 1 *[17] Assume that the function* $V : D \to R$ *is continuous and satisfies:*

(i) V *is positive definite.*

(ii) There are some real constants $c > 0$, $g \in [0, 1]$, $\alpha \in (0, 1)$, $0 < \varsigma < \infty$ *and an open region containing the origin* $U \subseteq D$ *such that:*

$$\dot{V}(x, t) \le -cV(x, t)^\alpha + \varsigma, x(t) \in U\backslash\{0\} \tag{13}$$

Then, the system reaches stability within finite time. The convergence time is given by:

$$T^* \le \frac{1}{cg(1-\alpha)}V^{1-\alpha}(x, 0). \tag{14}$$

Define the observation error as:

$$\begin{cases} \tilde{D}_m = D_m - \hat{D}_m \\ \tilde{D}_L = D_L - \hat{D}_L. \end{cases} \tag{15}$$

Substituting (15) into (3) gives:

$$\omega_L^{(3)} = -u + \Delta_o \tag{16}$$

where

$$\Delta_o = -\frac{K_s}{J_m J_L}\left(1+\frac{J_m}{J_L}\right)\tilde{D}_m + \frac{K_s}{J_m J_L}\frac{J_m}{J_L}\tilde{D}_L + \Delta_r \quad (17)$$

which is bounded and differentiable. Then, it follows that:

$$|\Delta_o| \leq \Delta_{\max}. \quad (18)$$

Theorem 2 *If the sliding surface (9) is selected, and the improved sliding mode reaching law (11) is adopted, then the control law (12) is asymptotically stable.*

Proof 2 *Define the Lyapunov function as follows:*

$$V_1 = \frac{1}{2}l_\omega^2. \quad (19)$$

Differentiating (19) gives

$$\begin{aligned}\dot{V}_1 &= l_\omega \dot{l}_\omega = -k_1|S_\omega|^{1-\alpha_1}|l_\omega|^{2-\alpha_1} - k_2|l_\omega|^{2+\alpha_1} + l_\omega\Delta_o \\ &\leq -k_1|S_\omega|^{1-\alpha_1}|l_\omega|^{2-\alpha_1} - k_2|l_\omega|^{2+\alpha_1}\Delta_{\max}|l_\omega| \\ &\leq -|l_\omega|\left[k_1|S_\omega|^{1-\alpha_1}|l_\omega|^{1-\alpha_1} + k_2|l_\omega|^{1+\alpha_1} - \Delta_{\max}\right]. \end{aligned} \quad (20)$$

Choose the width of the boundary layer:

$$k_1|S_\omega|^{1-\alpha_1}\delta_l^{1-\alpha_1} + k_2\delta_l^{1+\alpha_1} > \Delta_{\max}. \quad (21)$$

Then, when $|l_\omega| > \delta_l$, there is $\dot{V}_l < 0$. Thus, l_ω can enter the boundary layer in a finite time. If a constant $0 < \rho < 1$ is selected, and $\Delta_{\max} \leq \rho\left[k_1|S_\omega|^{1-\alpha_1}\delta_l^{1-\alpha_1} + k_2\delta_l^{1+\alpha_1}\right]$ is set, then when $|l_\omega| \geq \delta_l$, we have:

$$\dot{V}_1 \leq -(1-\rho)|l_\omega|\left[k_1|S_\omega|^{1-\alpha_1}|l_\omega|^{1-\alpha_1} + k_2|l_\omega|^{1+\alpha_1}\right]. \quad (22)$$

According to Lemma 1, the convergence time to the boundary layer, denoted by t_δ, is:

$$T_\delta \leq \frac{1}{(1-\rho)\lambda_2(1-\varepsilon)}\ln\left[\frac{\lambda_1 + \lambda_2|l_\omega(0)|^{1-\varepsilon}}{\lambda_1 + \lambda_2\delta_l^{1-\varepsilon}}\right]. \quad (23)$$

Moreover, under ideal observation and complete disturbance compensation conditions, that is, when $\Delta_0 = 0$, the convergence time of the outer sliding mode variable l_ω satisfies:

$$T_1 \leq \frac{1}{\lambda_2(1-\varepsilon)}\ln\left[1 + \frac{\lambda_2}{\lambda_1}|l_\omega(0)|^{1-\varepsilon}\right]. \quad (24)$$

Based on the definition of the l_ω sliding surface, when $\dot{l}_\omega = 0$, the following equation is obtained:

$$\ddot{S}_\omega + \gamma f_1(S_\omega) + \beta \mathrm{sign}(\dot{S}_\omega)|\dot{S}_\omega|^q = 0. \quad (25)$$

Let $x_1 = S_\omega$ and $x_2 = \dot{S}_\omega$. Then:

$$\begin{cases}\dot{x}_1 = x_2 \\ \dot{x}_2 = -\gamma f_1(x_1) - \beta\mathrm{sign}(x_2)|x_2|^q.\end{cases} \quad (26)$$

From Theorem 1, we know that $x_1 f_1(x_1) > 0$. If positive constants c_1, c_2 exist, then we have $c_1|x_1|^p \leq |f_1(x_1)| \leq c_2|x_1|^p$. Therefore, $f_1(x_1)$ is equivalent to $\mathrm{sign}(x_1)|x_1|^p$ over the entire error range, and system (26) can be regarded as a standard second-order terminal stable system:

$$\begin{cases}\dot{x}_1 = x_2 \\ \dot{x}_2 = -\gamma\mathrm{sign}(x_1)|x_1|^p - \beta\mathrm{sign}(x_2)|x_2|^{\frac{2p}{1+p}}.\end{cases} \quad (27)$$

Consider the Lyapunov function:

$$V_2 = \frac{1}{2}x_2^2 + \gamma\int_0^{x_1} f_1(t)dt. \quad (28)$$

Differentiating V_2 gives:

$$\begin{aligned}\dot{V}_2 &= x_2\dot{x}_2 + \gamma f_1(x_1)\dot{x}_1 \\ &= x_2\left[-\gamma f_1(x_1) - \beta\mathrm{sign}(x_2)|x_2|^q\right] + \gamma f_1(x_1)x_2 \\ &= -\gamma x_2 f_1(x_1) - \beta x_2\mathrm{sign}(x_2)|x_2|^q + \gamma x_2 f_1(x_1) \\ &= -\beta x_2\mathrm{sign}(x_2)|x_2|^q = -\beta|x_2|^{q+1} \leq 0.\end{aligned} \quad (29)$$

According to the LaSalle invariance principle, $x_1 \to 0$, $x_2 \to 0$, that is, $S_\omega \to 0$, $\dot{S}_\omega \to 0$. Since $q = \frac{2p}{1+p}$, system (27) is a negatively homogeneous system with homogeneity degree $k = \frac{p-1}{2} < 0$. According to the finite-time stability theorem for negative homogeneity [18], there exists a finite convergence time T_s such that $S_\omega(t) = 0$, $\dot{S}_\omega(t) = 0$, for $t \geq T_S$.

When $S_\omega = 0$, there is:

$$\dot{e}_\omega + c_1 e_\omega + c_2\int_0^t e_\omega(\tau)d\tau = 0. \quad (30)$$

Let $z_e = \int_0^t e_\omega(\tau)d\tau$. Then, $\dot{z}_e = e_\omega$. This can be expressed in the form of the following state-space equation:

$$\begin{bmatrix}\dot{e}_\omega \\ \dot{z}_e\end{bmatrix} = \begin{bmatrix}-c_1 & -c_2 \\ 1 & 0\end{bmatrix}\begin{bmatrix}e_\omega \\ z_e\end{bmatrix}. \quad (31)$$

The characteristic equation of (31) is obtained as:

$$s^2 + c_1 s + c_2 = 0. \quad (32)$$

According to the Hurwitz criterion, because $c_1 > 0$, $c_2 > 0$, the system is asymptotically stable. Therefore, the proposed control law is stable.

4. DESIGN OF DUAL FTESMDOS

This section presents dual FTESMDOs and analyzes their stability.

Considering the motor-side disturbance D_m an extended state, the augmented system can be expressed as follows:

$$\begin{bmatrix}\dot{\omega}_m \\ \dot{D}_m\end{bmatrix} = \begin{bmatrix}0 & -\frac{1}{J_m} \\ 0 & 0\end{bmatrix}\begin{bmatrix}\omega_m \\ D_m\end{bmatrix} + \begin{bmatrix}\frac{1}{J_m} \\ 0\end{bmatrix}T_e + \begin{bmatrix}0 \\ \Theta_s\end{bmatrix} \quad (33)$$

where Θ_s is the derivative of the shaft torque D_m, and both Θ_s and D_m are bounded.

According to Equation (33), the observer can be constructed as:

$$\begin{bmatrix}\dot{\hat{\omega}}_m \\ \dot{\hat{D}}_m\end{bmatrix} = \begin{bmatrix}0 & -\frac{1}{J_m} \\ 0 & 0\end{bmatrix}\begin{bmatrix}\hat{\omega}_m \\ \hat{D}_m\end{bmatrix} + \begin{bmatrix}\frac{1}{J_m} \\ 0\end{bmatrix}T_e + \begin{bmatrix}u_1 \\ l_1 u_1\end{bmatrix} \quad (34)$$

where $\hat{\omega}_m$ denotes the observation of ω_m; $\hat{D}_m$ denotes the estimate of D_m; l_1 represents the control gain; and u_1 represents the observer's SMC law.

Similarly, considering the load-side disturbance D_L an extended state, the augmented system can be expressed as follows:

$$\begin{bmatrix}\dot{\omega}_L\\ \dot{D}_L\end{bmatrix} = \begin{bmatrix}0 & -\frac{1}{J_L}\\ 0 & 0\end{bmatrix}\begin{bmatrix}\omega_L\\ D_L\end{bmatrix} + \begin{bmatrix}\frac{1}{J_L}\\ 0\end{bmatrix}T_s + \begin{bmatrix}0\\ \Theta_L\end{bmatrix} \tag{35}$$

where Θ_L is the derivative of the load side disturbance D_L, and both Θ_L and D_L are bounded.

According to Equation (35), the observer can be constructed as:

$$\begin{bmatrix}\dot{\hat{\omega}}_L\\ \dot{\hat{D}}_L\end{bmatrix} = \begin{bmatrix}0 & -\frac{1}{J_L}\\ 0 & 0\end{bmatrix}\begin{bmatrix}\hat{\omega}_L\\ \hat{D}_L\end{bmatrix} + \begin{bmatrix}\frac{1}{J_L}\\ 0\end{bmatrix}T_s + \begin{bmatrix}u_2\\ l_2u_2\end{bmatrix} \tag{36}$$

where $\hat{\omega}_L$ denotes the observation of ω_L; $\hat{D}_L$ denotes the estimate of D_L; l_2 represents the control gain; and u_2 represents the observer's SMC law.

The motor angular velocity estimation error e_m, estimation error e_1 of the motor side disturbance D_m, load angular velocity observation error e_L, and estimation error e_2 corresponding to the load disturbance D_L are expressed as:

$$\begin{cases} e_m = \omega_m - \hat{\omega}_m\\ e_1 = D_m - \hat{D}_m\\ e_L = \omega_L - \hat{\omega}_L\\ e_2 = D_L - \hat{D}_L. \end{cases} \tag{37}$$

From Assumption 2, e_1 and e_2 have upper bounds $D_{1\max}$ and $D_{2\max}$, respectively, namely $|e_1| \le D_{1\max}$ and $|e_2| \le D_{2\max}$.

By combining (33) to (36), the error dynamic equations of the dual observers are obtained as follows:

$$\begin{cases} \dot{e}_m = -\frac{1}{J_m}e_1 - u_1\dot{e}_1 = \Theta_m - l_1u_1\\ \dot{e}_L = -\frac{1}{J_L}e_2 - u_2\dot{e}_2 = \Theta_L - l_2u_2. \end{cases} \tag{38}$$

Select sliding surfaces s_m and s_L as:

$$\begin{cases} s_m = e_m + c_{m1}\int_0^t e_m dt + c_{m2}\int_0^t \mathrm{sign(e_m)|e_m|^{r_1}dt}\\ s_L = e_L + c_{L1}\int_0^t e_L dt + c_{L2}\int_0^t \mathrm{sign(e_L)|e_L|^{r_2}dt}. \end{cases} \tag{39}$$

From Equations (33) to (39), it follows that:

$$\begin{cases} \dot{s}_m = -\frac{1}{J_m}e_1 - u_1 + c_{m1}e_m + c_{m2}\mathrm{sign(e_m)|e_m|^{r_1}}\\ \dot{s}_L = -\frac{1}{J_L}e_2 - u_2 + c_{L1}e_L + c_{L2}\mathrm{sign(e_L)|e_L|^{r_2}}. \end{cases} \tag{40}$$

where $c_{m1} > 0$, $c_{m2} > 0$, $c_{L1} > 0$, $c_{L2} > 0$, $0 < r_1 < 1$, $0 < r_2 < 1$.

Select the double power reaching law as:

$$\begin{cases} \dot{s}_m = u_m = -k_{m1}(|e_m||s_m|)^{1-\alpha_m}\mathrm{sign(s_m)}\\ \qquad -k_{m2}|s_m|^{1+\alpha_m}\mathrm{sign(s_m)} - \mathrm{k_{m3}sign(s_m)}\\ \dot{s}_L = u_L = -k_{L1}(|e_l||s_L|)^{1-\alpha_L}\mathrm{sign(s_L)}\\ \qquad -k_{L2}|s_L|^{1+\alpha_L}\mathrm{sign(s_L)} - \mathrm{k_{L3}sign(s_L)} \end{cases} \tag{41}$$

where $0 < \alpha_m < 1$, $k_{m1} > 0$, $k_{m2} > 0$, $k_{m3} > 0$, $0 < \alpha_L < 1$, $k_{L1} > 0$, $k_{L2} > 0$, and $k_{L3} > 0$ are parameters to be designed.

By combining (39) and (40), the SMC law is obtained as follows:

$$\begin{cases} u_1 = c_{m1}e_m + c_{m2}\mathrm{sign(e_m)|e_m|^{r_1} - u_m}\\ u_2 = c_{L1}e_L + c_{L2}\mathrm{sign(e_L)|e_L|^{r_2} - u_L} \end{cases} \tag{42}$$

Theorem 3 *Select sliding surfaces (39), dual power reaching law (41), and design the control law (42). When the system gains satisfy (43), error dynamics converge to the sliding surface in finite time, and the disturbance estimation errors become bounded after finite time.*

$$\begin{cases} k_{m3} > \frac{D_{1\max}}{J_m}, \quad l_1 < 0\\ k_{L3} > \frac{D_{2\max}}{J_L}, \quad l_2 < 0. \end{cases} \tag{43}$$

Proof 3 *Define the Lyapunov function as follows:*

$$V_3 = 0.5s_m^2 \tag{44}$$
$$V_4 = 0.5s_L^2. \tag{45}$$

Differentiating V_3 with respect to time gives:

$$\begin{aligned} \dot{V}_3 &= s_m\dot{s}_m\\ &= s_m\left[-\frac{1}{J_m}e_1 - u_1 + c_{m1}e_m + c_{m2}\mathrm{sig^{r_1}(e_m)}\right]\\ &= -k_{m3}|s_m| - \frac{1}{J_m}s_me_1 \le -\left(k_{m3} - \frac{D_{1\max}}{J_m}\right)|s_m|. \end{aligned}$$

To ensure $\dot{V}_3 \le 0$, parameter k_{m3} must satisfy:

$$k_{m3} > \frac{D_{1\max}}{J_m} \tag{46}$$

such that

$$e_1(t)| \le \rho_1, \quad \mathit{for} \quad t \ge t_m. \tag{47}$$

To ensure the convergence of the disturbance estimation error, parameter l_1 must be selected as a negative value. Thus, the speed observation error on the motor side converges within a finite time t_m. When $\Theta_m = 0$ or $\Theta_m \to 0$, the disturbance estimation error converges to zero.

Similarly, differentiating (45) gives:

$$\dot{V}_4 = s_L\dot{s}_L \le -\left(k_{L3} - \frac{D_{2\max}}{J_L}\right)|s_L|. \tag{48}$$

To ensure $\dot{V}_4 \le 0$, parameter k_{L2} must satisfy:

$$k_{L3} > \frac{D_{2\max}}{J_L}. \tag{49}$$

Thus, the observer (36) is asymptotically stable, and the system state can reach the sliding surface in finite time t_{s2}. From $s_L = \dot{s}_L = 0$, it follows that $e_L = \dot{e}_L = 0$. At this point,

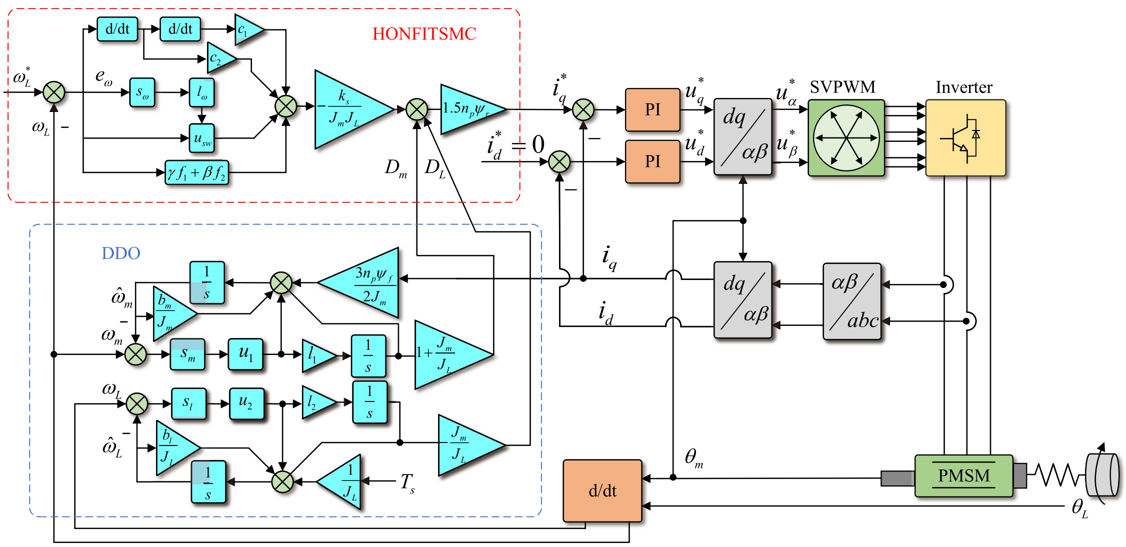

FIGURE 3. Block diagram of the PMSM dual-inertia system.

TABLE 1. System parameters.

Parameters	Value	Unit
DC link voltage (U_{dc})	350	V
Rotor PM flux (ψ_r)	0.171	Wb
Stator inductance (L)	0.00334	H
Number of pole pairs (n_p)	4	–
Stator resistance (R_s)	1.9	Ω
Rotational Inertia (J_m)	0.025	kg m^2
Load inertia (J_L)	0.15	kg m^2
Torsional damping (b_s)	0.8	N m s rad^{-1}
Stiffness coefficient (K_s)	415	N m rad^{-1}

TABLE 2. Parameters of control schemes.

PI	NFTSMC	HONFITSMC
$k_p = 1.75$	$\alpha = 12000$	$c_1 = 90, c_2 = 2500$
$k_i = 20$	$\beta = 2000$	$q = 0.82, \alpha_1 = p = 0.8$
–	$l/h = 7/3$	$k_1 = 1.5, k_2 = 500$
–	$p/q = 5/3$	$c_{m1} = 100, c_{L1} = 100$
–	$\varepsilon = 0.01$	$c_{m2} = 50, c_{L2} = 75$
–	$k = 0.008$	$r_m = r_l = 7/9, \alpha_m = \alpha_L = 0.8$
–	$\gamma = 200$	$l_1 = -30, l_2 = -50$
–	$\eta = 4000$	$k_{m1} = 50, k_{L1} = 75$
–	$l_1 = 62$	$k_{m2} = 100, k_{L2} = 300$
–	–	$k_{m3} = 60, k_{L3} = 250$

$\dot{e}_L$ and $\dot{e}_2$ (33) can be simplified as $\dot{e}_2 = \Theta_L + \frac{l_2}{J_L} e_2$. Since $|\Theta_L| \leq \bar{\Theta}_L$, for any $\rho_2 > \frac{\bar{\Theta}_L}{a_L}$, where $a_L = -\frac{l_2}{J_L} > 0$, we have

$$e_2(t)| \leq |e_2(t_s)| e^{-a_L(t-t_{s2})} + \frac{\bar{\Theta}_L}{a_L}\left(1 - e^{-a_L(t-t_{s2})}\right). \quad (50)$$

Then, there exists

$$t_L \leq t_{s2} + \frac{1}{a_L} \ln \frac{|e_2(t_{s2})| - \frac{\bar{\Theta}_L}{a_L}}{\rho_2 - \frac{\bar{\Theta}_L}{a_L}} \quad (51)$$

such that

$$e_2(t)| \leq \rho_2, \quad for \quad t \geq t_L. \quad (52)$$

To ensure convergence of the disturbance estimation error, l_2 must be selected as a negative value. Thus, the speed observation error on the load side converges within a finite time t_L. When $\Theta_L = 0$ or $\Theta_L \to 0$, the disturbance estimation error further converges to zero.

To suppress high-frequency chattering, the conventional sign function was replaced by a saturation function. The saturation function sat is defined as follows:

$$\text{sat(s)} = \begin{cases} 1 & s > \sigma \\ s/\sigma & -\sigma \leq s \leq \sigma \\ -1 & s < -\sigma \end{cases} \quad (53)$$

where σ denotes the transition layer. Linear feedback control is used inside this layer, whereas switching control is applied outside it.

Figure 3 shows the structural diagram of the proposed HONFITSMC torsional vibration suppression system.

5. SIMULATION AND EXPERIMENTATION

5.1. Simulation Results and Analysis

Table 1 provides system parameters. Table 2 lists the parameters of control schemes. The PMSM operates using the $i_d = 0$ vector control strategy. The sampling interval is set to 0.00001 s, and the DC link voltage of the three-phase inverter is $U_{\text{dc}} = 350$ V. The presented HONFITSMC approach is then evaluated against the PI and ESMDO-based NFTSMC algorithms.

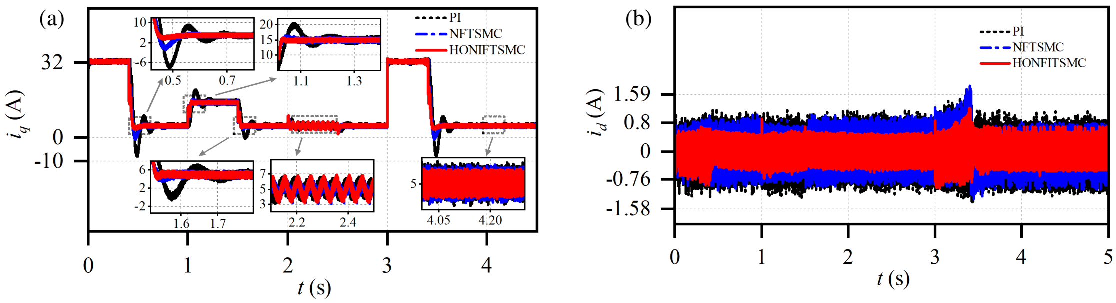

FIGURE 4. d-q axis current response. (a) q-axis current response and (b) d-axis current response.

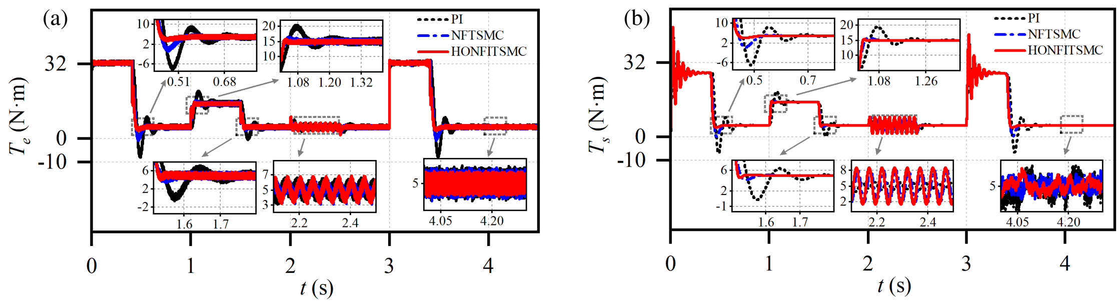

FIGURE 5. Electromagnetic torque and shaft torque. (a) Electromagnetic torque response and (b) shaft torque response.

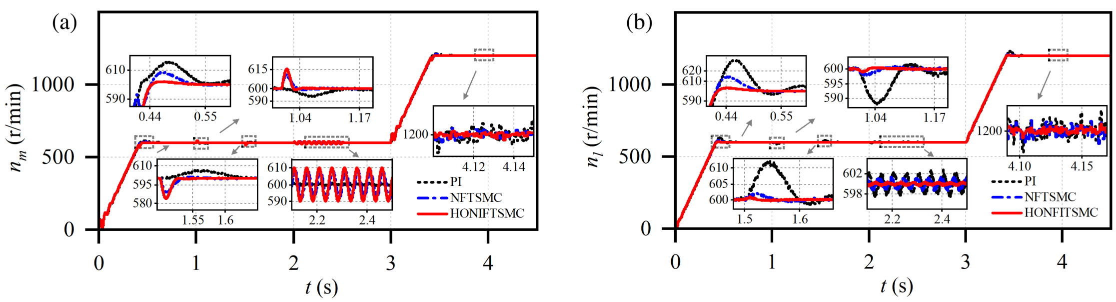

FIGURE 6. Speed response on motor and load sides. (a) Speed response of the motor side and (b) speed response of the load side.

The initial load torque is set to $T_L = 5\,\mathrm{N{\cdot}m}$. At 0 s, the inductance, resistance, motor inertia, and viscous friction coefficient are increased by factors of 1.02, 1.12, 1.4, and 3, respectively. External disturbances are applied as follows:

- at 3 s, the motor speed increases from 600 r/min to 1200 r/min;
- at 1 s, a load torque of 10 N·m is suddenly applied;
- at 1.5 s, the 10 N·m load torque is suddenly removed;
- at 2 s, a sinusoidal disturbance of $5\sin(40\omega t)$ is introduced.

Figures 4(a), 4(b), 5(a), and 5(b) present the q-axis current, d-axis current, electromagnetic torque, and shaft torque responses, respectively. Compared with PI and NFTSMC, HONFITSMC produced smaller ripple in d- and q-axis currents and electromagnetic torque during steady-state operation. It also provides smoother shaft torque responses during step changes in speed. Although all three methods generate transient shaft torque fluctuations, HONFITSMC suppresses torsional vibration more rapidly and enables the shaft torque to approach its steady-state value more smoothly.

Under periodic disturbances, the low bandwidth of PI control limits its response to high-frequency disturbances. Thus, PI control produces relatively small shaft torque fluctuations, but its speed-tracking and disturbance-recovery performance are poor. NFTSMC and HONFITSMC respond more effectively to disturbances and provide stronger compensation. Compared with NFTSMC, HONFITSMC produces a smoother shaft torque response while maintaining strong disturbance compensation. Therefore, HONFITSMC achieves a better balance between disturbance compensation and torsional vibration suppression.

Figures 6(a) and 6(b) present speed responses on motor and load sides. Sudden changes in the speed reference or load torque induce torsional vibrations on both sides, which arise from the dynamic response of the elastic shaft. The results were as follows:

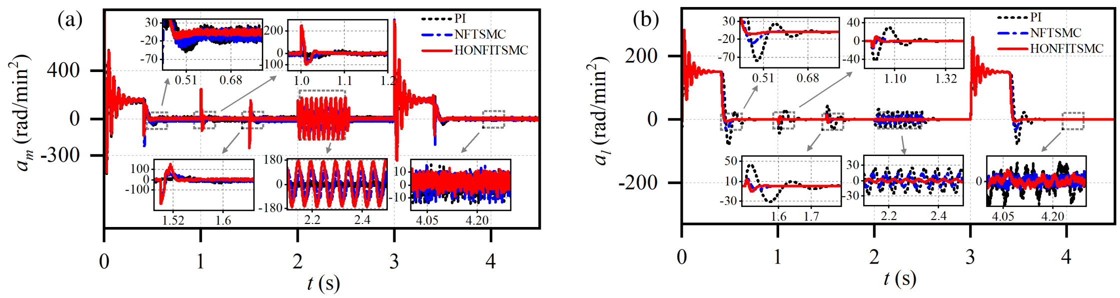

FIGURE 7. Acceleration response on the motor and load sides. (a) Acceleration of the motor side and (b) acceleration of the load side.

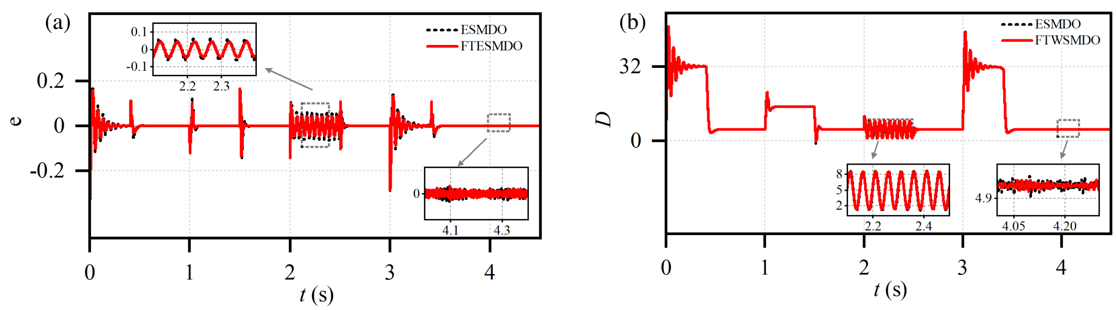

FIGURE 8. Speed tracking error and observed disturbance. (a) Speed tracking error and (b) observed disturbance.

(i) Under PI control, the load speed follows the reference signal within 0.7 s, with an overshoot of approximately 5%. The NFTSMC tracked the reference signal within 0.54 s, with an overshoot of approximately 2.5%. In contrast, HONFITSMC achieved tracking without a steady-state error within 0.5 s, with an overshoot of only 0.83%.

(ii) At 1 s, a sudden load was applied, and at 1.5 s, it was removed. Under both conditions, PI control produced a load-speed deviation of approximately 12 r/min, with a recovery time of approximately about 0.3 s. NFTSMC reduced the speed deviation to approximately 3 r/min and the recovery time to approximately about 0.1 s. HONFITSMC further reduced the deviation to approximately 1 r/min and provided the fastest recovery. However, the motor speed exhibited a reverse overshoot under NFTSMC and HONFITSMC.

(iii) At 2 s, when a sudden sinusoidal load disturbance is applied, PI control shows speed fluctuations of about 3 r/min. The NFTSMC method shows speed fluctuations of about 1 r/min, while the HONFITSMC method shows only 0.2 r/min speed fluctuation.

(iv) In summary, compared with PI and NFTSMC, the HONFITSMC method achieves faster load-side response speed, smaller overshoot, and better disturbance rejection capability. The HONFITSMC and NFTSMC control methods using load-speed feedback and sliding-mode algorithms can effectively suppress torsional vibration.

Figures 7(a) and 7(b) present angular acceleration responses on the motor-side and load-side, respectively. Compared with PI and NFTSMC methods, HONFITSMC produced smaller acceleration fluctuations and shorter settling times on both sides, improving the stability of the dual-inertia system.

Figures 8(a) and 8(b) present speed estimation errors and disturbance estimates obtained using ESMDO and FTESMDO, respectively. Both observers provided satisfactory estimation performance. Compared with ESMDO, FTESMDO produced less chattering in estimated signals, improving the robustness and disturbance rejection of the dual-inertia system.

5.2. Experimental Results and Analysis

Figure 9 shows an RT-LAB (OP5600) experimental platform, which is mainly composed of a host computer, digital signal processing (DSP), and OP5600. TMS230F2812 is the DSP's control chip, and RT-LAB (OP5600) simulates the PMSM dual-inertia system. The experimental and simulated parameters are kept consistent.

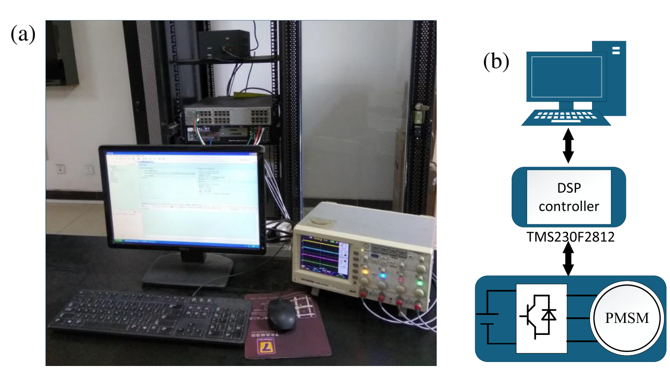

FIGURE 9. RT-LAB HILS experiment platform. (a) RT-LAB platform and (b) configuration.

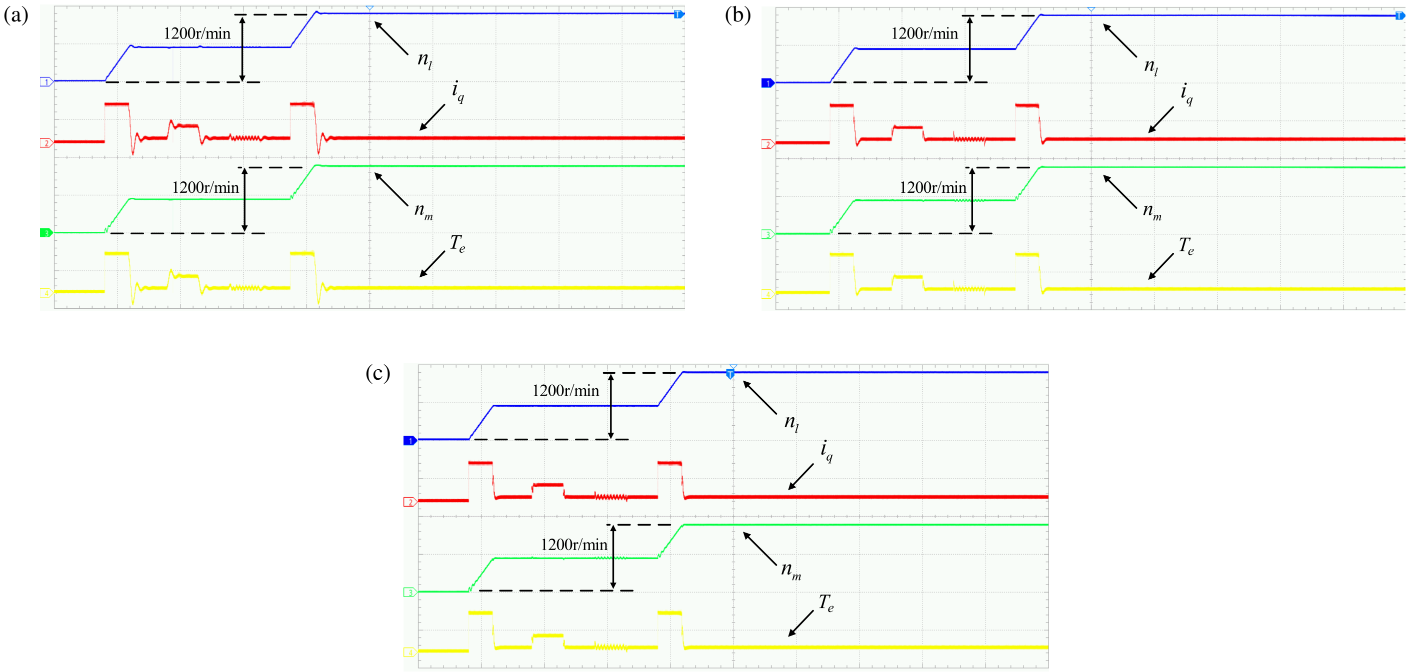

FIGURE 10. Experimental waveforms of the current, speed, and torque. (a) PI control, (b) NFTSMC, and (c) HONFITSMC.

Figure 10 shows experimental results of the three methods: PI, NFTSMC, and HONFITSMC. It can be concluded that:

(i) For abrupt changes in the load speed reference and load torque, the proposed HONFITSMC method achieves the fastest load speed response and smallest steady-state error among the compared methods.

(ii) In the case of periodic disturbances, both PI control and NFTSMC show limited disturbance rejection and slower convergence speed. In contrast, HONFITSMC effectively suppresses load-side torsional vibration, maintains accurate and stable load speed tracking, produces a more stable output torque, and achieves excellent dynamic and steady-state performance.

6. CONCLUSION

To address problems in load speed tracking, flexible shaft torsional vibration, and load-disturbance suppression in PMSM dual-inertia flexible transmission systems, this paper proposes a dual FTESMDOs-based HONFITSMC method. The main conclusions are as follows:

(i) The third-order load-side dynamic model of a PMSM dual-inertia flexible drive system was established. An HONFITSMC controller was designed, by which a good trade-off between the system convergence speed and chattering suppression was achieved. The load speed tracking performance was also improved.

(ii) Dual FTESMDOs were designed for motor and load sides. Shaft torque and load disturbance were estimated using two observers. Feedforward compensation was provided for the control law using estimated values. Consequently, the system robustness against disturbances from both the flexible shaft and external sources was enhanced.

(iii) The comprehensive comparison of simulated and experimental results shows that the proposed method exhibits good control performance in load speed tracking, disturbance suppression, and torsional vibration reduction.

ACKNOWLEDGEMENT

This work was supported in part by the National Natural Science Foundation of China under Grants 52572375 and 62303178 and the Hunan Provincial Natural Science Foundation of China under Grants 2026JJ80067 and 2026JJ90264.

REFERENCES

[1] Zheng, L., J. Liu, S. Li, Y. Ding, Q. Guan, and X. Wang, "High-performance control strategy for robot servo system with flexible joint via output regulation model predictive control," *IEEE Transactions on Power Electronics*, Vol. 41, No. 4, 5237–5248, April 2026.

[2] You, X., K. H. Zhao, Y. Y. Lu, M. J. Qiao, J. Y. Huang, and X. F. Li, "Distributed speed collaborative sliding mode control for high-speed trains based on extended sliding mode disturbance observer," *Journal of Hunan University of Technology*, Vol. 39, No. 1, 43–50, 2025.

[3] Wang, B., M. Tian, Y. Yu, Q. Dong, and D. Xu, "Enhanced ADRC with quasi-resonant control for PMSM speed regulation considering aperiodic and periodic disturbances," *IEEE Transactions on Transportation Electrification*, Vol. 8, No. 3, 3568–3577, September 2022.

[4] Han, X., X. Chen, F. Zheng, and L. Hua, "An adaptive PI control method considering large inertia for multi-DoF forming robot," *IEEE Transactions on Instrumentation and Measurement*, Vol. 74, 1–12, November 2025.

[5] Qiao, M., K. Zhao, B. Fang, J. She, and Y. Huang, "Model-free fast integral terminal sliding mode control based on extended super-twisting sliding mode disturbance observer for PMSM with unknown disturbances," *International Journal of Circuit Theory and Applications*, Vol. 54, No. 3, 1572–1583, July 2025.

[6] Xia, J. and H. Ouyang, "Chattering free sliding-mode controller design for underactuated tower cranes with uncertain disturbance," *IEEE Transactions on Industrial Electronics*, Vol. 71, No. 5, 4963–4975, May 2024.

[7] Zhihong, M., A. P. Paplinski, and H. R. Wu, "A robust MIMO terminal sliding mode control scheme for rigid robotic manipulators," *IEEE Transactions on Automatic Control*, Vol. 39, No. 12, 2464–2469, December 1994.

[8] Feng, Y., X. Yu, and Z. Man, "Non-singular terminal sliding mode control of rigid manipulators," *Automatica*, Vol. 38, No. 12, 2159–2167, December 2002.

[9] Xu, W., S. Qu, and C. Zhang, "Fast terminal sliding mode current control with adaptive extended state disturbance observer for PMSM system," *IEEE Journal of Emerging and Selected Topics in Power Electronics*, Vol. 11, No. 1, 418–431, February 2023.

[10] Liang, Z., Q. Gao, M. Shen, J. Liu, J. Gao, Y. Hu, and J. Zhao, "Adaptive integral terminal sliding mode control to improve maneuverability of electric vehicle considering rollover and inputs saturation," *IEEE Transactions on Transportation Electrification*, Vol. 11, No. 2, 6012–6024, April 2025.

[11] Yang, T., Y. Deng, H. Li, Z. Sun, H. Cao, and Z. Wei, "Fast integral terminal sliding mode control with a novel disturbance observer based on iterative learning for speed control of PMSM," *ISA Transactions*, Vol. 134, 460–471, March 2023.

[12] Lu, Y., K. Zhao, X. You, M. Qiao, Y. He, and L. Tu, "Model-free recursive terminal sliding mode control for a permanent magnet synchronous motor dual inertia system based on a double disturbance observer," *Power System Protection and Control*, Vol. 52, No. 21, 129–139, 2024.

[13] Fu, X. and J. Xiong, "Multielement disturbance observer for separately estimating periodic and nonperiodic disturbances in PMSM control systems," *IEEE Transactions on Power Electronics*, Vol. 41, No. 3, 3388–3398, March 2026.

[14] Han, J., "From PID to active disturbance rejection control," *IEEE Transactions on Industrial Electronics*, Vol. 56, No. 3, 900–906, March 2009.

[15] Zhao, K., W. Dai, R. Zhou, A. Leng, W. Liu, P. Qiu, G. Huang, and G. Wu, "Novel model-free sliding mode control of permanent magnet synchronous motor based on extended sliding mode disturbance observer," *Proceedings of the CSEE*, Vol. 42, No. 6, 2375–2386, 2022.

[16] Guo, X., S. D. Huang, Y. Peng, J. Y. Yang, and H. X. Wang, "Sliding mode control of IPMSM speed regulation system based on an improved double power reaching law and global fast terminal sliding mode observer," *Transactions of China Electrotechnical Society*, Vol. 38, No. 1, 190–203, 2023.

[17] Wang, H., P. X. Liu, X. Zhao, and X. Liu, "Adaptive fuzzy finite-time control of nonlinear systems with actuator faults," *IEEE Transactions on Cybernetics*, Vol. 50, No. 5, 1786–1797, May 2020.

[18] Bhat, S. P. and D. S. Bernstein, "Geometric homogeneity with applications to finite-time stability," *Mathematics of Control, Signals, and Systems*, Vol. 17, No. 2, 101–127, May 2005.